AIP | Conference Proceedings

Long Range Interactions in MagnetoOptical Traps

G. Labeyrie, G. L. Gattobigio, T. Pohl, and R. Kaiser

Citation: AIP Conf. Proc. **970**, 303 (2008); doi: 10.1063/1.2839128
View online: http://dx.doi.org/10.1063/1.2839128
View Table of Contents: http://proceedings.aip.org/dbt/dbt.jsp?KEY=APCPCS&Volume=970&Issue=1
Published by the AIP Publishing LLC.

Additional information on AIP Conf. Proc.

Journal Homepage: http://proceedings.aip.org/
Journal Information: http://proceedings.aip.org/about/about_the_proceedings
Top downloads: http://proceedings.aip.org/dbt/most_downloaded.jsp?KEY=APCPCS
Information for Authors: http://proceedings.aip.org/authors/information_for_authors

ADVERTISEMENT

Downloaded 16 Jul 2013 to 193.48.228.35. This article is copyrighted as indicated in the abstract. Reuse of AIP content is subject to the terms at: http://proceedings.aip.org/about/rights_permissions

Long Range Interactions in Magneto-Optical Traps

G. Labeyrie*, G. L. Gattobigio*, T. Pohl† and R. Kaiser*

*Institut Non Linéaire de Nice, UMR 6618 CNRS, 1361 route des Lucioles, 06560 Valbonne, France.
†ITAMP, Harvard Smithsonian Center for Astrophysics, 60 Garden Street, Cambridge MA 02138.

Abstract.
We present in this paper a review of our work on the impact of long-range interactions on the static and dynamic behaviors of magneto-optical traps (MOT) for neutral atoms. In such systems, all forces (confinement and interaction) are mediated by light. The most obvious signature of long-range interactions is the dependence of the MOT size with number N of trapped atoms. We study in detail the scaling laws for the MOT size versus N, in a range of large $N \gg 10^8$. We then show that the competition between confinement and repulsive interaction can lead, for N large, to a new dynamical instability characterized by spontaneous, self-sustained oscillations of the MOT. This instability is investigated experimentally and theoretically, using both a simple analytical model and a more refined numerical one.

INTRODUCTION

Many-body systems with long-range interactions are present everywhere in nature. Understanding their properties is relevant for biology, physics, economy, ... and applies to issues as diverse as e.g. stellar pulsation [1], swarm dynamics [2] and instabilities in plasmas [3].

Among the great variety of systems belonging to this category, ensembles of very cold particles have recently emerged. Large samples of ions can be trapped and laser-cooled, yielding beautiful examples of crystallization due to the strong Coulomb interaction [4]. Ultra-cold plasmas can also be created by ionizing a cloud of laser-cooled atoms [5]. However, long-range interactions may also appear in ensembles of *neutral* atoms. Signatures of the magnetic dipole-dipole interaction have been recently obtained in a Bose-Einstein condensate of Chromium [6]. In the magneto-optical trap, the work horse of most cold atoms experiments nowadays, the re-absorption of scattered photons induces a Coulomb-like repulsive interaction [7].

In this paper, we focus on the later example and investigate the impact of light-induced long-range interactions on the static and dynamic behavior of the MOT. In particular we show that the MOT, under certain circumstances, develops a dynamical instability characterized by spontaneous, self-sustained radial oscillations. These are reminiscent of pulsating stars [1], where the regular oscillation of the star diameter is due to a competition between the compression force of gravity and the outwards-directed radiation pressure. In our system, both the confining force and the long-range interaction are mediated by light. The MOT is a nice tool where a high degree of control and tuning

CP970, *Dynamics and Thermodynamics of Systems with Long-range Interaction: Theory and Experiments*
edited by A. Campa, A. Giansanti, G. Morigi, and F. Sylos Labini
© 2008 American Institute of Physics 978-0-7354-0488-5/08/$23.00

wnloaded 16 Jul 2013 to 193.48.228.35. This article is copyrighted as indicated in the abstract. Reuse of AIP content is subject to the terms at: http://proceedings.aip.org/about/rights_permissi

capabilities are possible. It may thus prove an interesting model system to study related phenomena in astrophysics and plasma physics.

This paper is organized as follows. We first describe in the following section the experimental setup and the characterization techniques employed throughout this work. We then address the question of the scaling laws for the MOT size. The next section is devoted to the study of the dynamical instability observed in large MOTs.

EXPERIMENTAL TECHNIQUES

We describe in this section the experimental apparatus and the various techniques employed to produce, control and characterize the MOT.

Our magneto-optical trap is directly loaded from a dilute, room-temperature Rubidium vapor. In such a case, the number N of trapped atoms increases rapidly with the diameter of the trapping beams[8] provided that a laser intensity of the order of the Rb saturation intensity (1.4 mW/cm^2) can be sustained. Thus, we employ 6 large *independent* trapping beams ($1/e^2$ radius 4 cm) of power 30 mW each. The laser power (total 180 mW in the MOT, after spatial filtering) is obtained by single-pass amplification of a narrow line ($\approx$ 2 MHz) master DBR laser through a tapered amplifier. The trapping and cooling force is obtained by illuminating the Rb^{85} atoms with the six beams arranged in three orthogonal counter-propagating pairs. This configuration is fully symmetric, as opposed to the traditional choice of three retro-reflected beams where the shadow effect can imbalance the forces acting on the atoms and yield a dynamical instability characterized by oscillation of the center-of-mass of the MOT[9]. A 3D gradient of magnetic field, necessary to introduce a position-dependent restoring component in the force exerted by the laser beams, is generated by a pair of coils in anti-Helmoltz configuration. The magnitude of this gradient is typically 10 G/cm.

Figure 1 shows a simplified energy diagram of the D2 line employed for the trapping of Rb^{85}. The trapping light is tuned slightly below the $F = 3 \rightarrow F' = 4$ transition. The MOT detuning $\delta = \omega - \omega_{at}$ is typically -3Γ (ω and ω_{at} are the laser and atomic resonance angular frequencies respectively, and $\Gamma = 2\pi \times 6$ MHz is the natural width of the atomic transition). This atomic transition is closed since the atom can not decay in another ground state, i.e. $F = 2$. However, the presence of other excited states like $F' = 3$ and 2 (not shown) allows for some leakage towards $F = 2$, albeit with a small probability due to the large detuning for the corresponding transitions. As a result, an atom exposed to the trapping light alone will scatter ≈ 1000 photons before being optically pumped into $F = 2$, where the interaction with the light will cease. The solution to circumvent this problem is to add a second, "repumper" laser tuned to resonance with e.g. the $F = 2 \rightarrow F' = 3$ transition. The effect of this laser is to efficiently pump the atoms in $F = 2$ back into $F = 3$. In our setup the repumper beam is retro-reflected and applied to the atoms along an axis different from that of the trapping beams.

It is important for our purpose to achieve a reliable and accurate characterization of the MOT: size, number of atoms, density ... This is done in the following way: prior to the measurement, we switch off the MOT (trapping and repumper beams, magnetic gradient). For large MOTs ($\approx$ 1 cm) the Zeeman shift may affect the shape of the fluorescence image, the magnetic field gradient must thus be switched off. We then illuminate

wnloaded 16 Jul 2013 to 193.48.228.35. This article is copyrighted as indicated in the abstract. Reuse of AIP content is subject to the terms at: http://proceedings.aip.org/about/rights_permissi

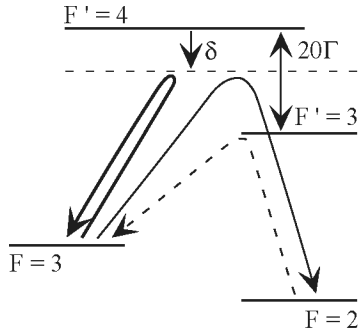

FIGURE 1. Level scheme relevant for MOT operation. The trapping light (bold arrow) is detuned slightly to the red of the $F = 3 \rightarrow F' = 4$ cycling transition of Rb^{85}. However, the off-resonant excitation of $F' = 3$ yields hyperfine pumping into the $F = 2$ "dark" state (thin arrow). This is avoided by adding a repumping laser tuned to resonance with the $F = 2 \rightarrow F' = 3$ transition (dashed arrow).

the cloud of atoms with a short (10 μs) pulse of the 6 trapping beams, but with a larger detuning $|\delta| > 6\Gamma$. Images of the scattered light distribution taken from 2 orthogonal directions are collected on a CCD camera. Because of the large detuning, the cloud of cold atoms is optically-thin i.e. in the single-scattering regime: the probability that a photon is scattered twice before leaving the cloud is very small. Thus, the images recorded on the CCD provide a reliable information on the 3D atomic density distributions (integrated along the line of sight). To obtain the number of trapped atoms N, we measure the optical thickness b of the cloud by monitoring the transmission of a probe beam through its center. Measuring the detuning dependence of this transmission allows to determine optical thicknesses up to large values [10]. Combining the optical thickness (integrated column density) measurement and the images of the density distribution we can extract the total number of atoms N, the density n and the *rms* size R of the cloud. An alternative way to obtain these parameters would be to use absorption imaging with a detuned probe. We stress that these precautions are necessary in the regime of large MOTs where the optical thickness of the cloud at the frequency of the trapping lasers is larger than unity. In this regime, monitoring the MOT fluorescence to deduce atomic density distributions, as done in previous studies, is likely to introduce systematic errors.

The setup described above produces MOTs with at most 2×10^{10} Rb^{85} atoms. The typical MOT size is 6 mm FWHM ($R \approx 2.5$ mm) with a maximum density $n \approx 2 \times 10^{10}$ cm^{-3}. The corresponding maximal optical thickness (for resonant light) is 40. The residual velocity is ≈ 10 cm/s, with a temperature in the 100 μK range. In the following, we will study various static and dynamical properties of the MOT as a function of the number of atoms N. This number can be varied using different methods. A simple one consists in varying the intensity of the repumping laser. This modifies the population in the "bright" state $F = 3$ and thus the average magneto-optical force acting on the atoms. As a consequence the MOT's capture velocity v_c is affected and accordingly the number of trapped atoms which scales as v_c^4 [8]. The drawback of this method is that p might also affect the physics we want to study, as will be seen in the next section. A cleaner

wnloaded 16 Jul 2013 to 193.48.228.35. This article is copyrighted as indicated in the abstract. Reuse of AIP content is subject to the terms at: http://proceedings.aip.org/about/rights_permissi

way to vary N is thus to adjust the *diameter* of the repumping (or trapping) beam, which also affects v_c. This in principle should not modify the parameters of the MOT. An alternative method (not steady-state) is to start with a MOT switched off, turn it on and adjust the duration of the loading before measuring. The MOT loads exponentially from the ambient vapor, with a time constant τ_{load} determined by the ambient Rb pressure. This technique can thus be employed if the measurement time, i.e. the typical time scale of the physics under study, is much smaller than τ_{load}.

MOT SIZE: SCALING LAWS

The effect of multiple scattering of light in the MOT was soon recognized after the first realization[11], since it was identified as the factor limiting the atomic density in traps with "large" numbers of atoms[7]. An important effort was developed to circumvent this problem, with techniques such as e.g. the "Dark Spontaneous Force Trap" allowing to gain a substantial factor on the density[12]. Even higher densities, required to achieve Bose-Einstein condensation, were obtained with the help of alternative cooling methods working without the presence of near-resonant light[13].

Basically, two regimes have been identified so far for the MOT: the temperature-limited regime and the multiple scattering regime. At low number N of trapped atoms ($N < 10^4$), these can be considered independent and the MOT size is determined by the equipartition between kinetic and potential energy:

$$R = \sqrt{k_B T / \kappa}\,, \tag{1}$$

where κ is the spring constant of the trap and T the temperature derived from the velocity dispersion. In this regime, the MOT size is independent of N.

For larger N the atomic cloud becomes optically-thick, with two consequences. First, the trapping light is attenuated after passing through the cloud, which tends to compress the MOT since the radiation pressure is stronger at the edges than near the center[14]. This compression force is proportional to $\langle\sigma_L\rangle^2$, where $\langle\sigma_L\rangle$ is the average absorption cross-section for a trapping laser photon. Second, a trapping photon scattered by an atom is likely to be re-absorbed by another, nearby atom. This results in a repulsive interaction between the two atoms with a Coulomb-like $1/r^2$ long-range dependence [7]. This $1/r^2$ dependence is due to the decrease of the intensity of the spherical wave radiated by the first atom. The repulsive force is proportional to the product $\langle\sigma_L\rangle\langle\sigma_R\rangle$, where $\langle\sigma_R\rangle$ is the absorption cross-section for a *scattered* photon. The *effective charge* for this Coulomb-like interaction is $\approx 5\times10^{-3}e$, for typical parameters. Our system is thus much less interacting than e.g. trapped ions, where crystallization (i.e. regular self-ordering due to the repulsive interaction) occurs [4]. In general, $\langle\sigma_L\rangle \neq \langle\sigma_R\rangle$ because photon scattering is inelastic for the standard parameters in a MOT. Due to this inelastic scattering, one has $\langle\sigma_R\rangle > \langle\sigma_L\rangle$, which implies that the *net* force (compression + repulsion) is repulsive [7]. The total force can be written as a function of the distance from trap center r under the form:

$$F(r) = -\kappa r + G_3 n r\,. \tag{2}$$

wnloaded 16 Jul 2013 to 193.48.228.35. This article is copyrighted as indicated in the abstract. Reuse of AIP content is subject to the terms at: http://proceedings.aip.org/about/rights_permissi

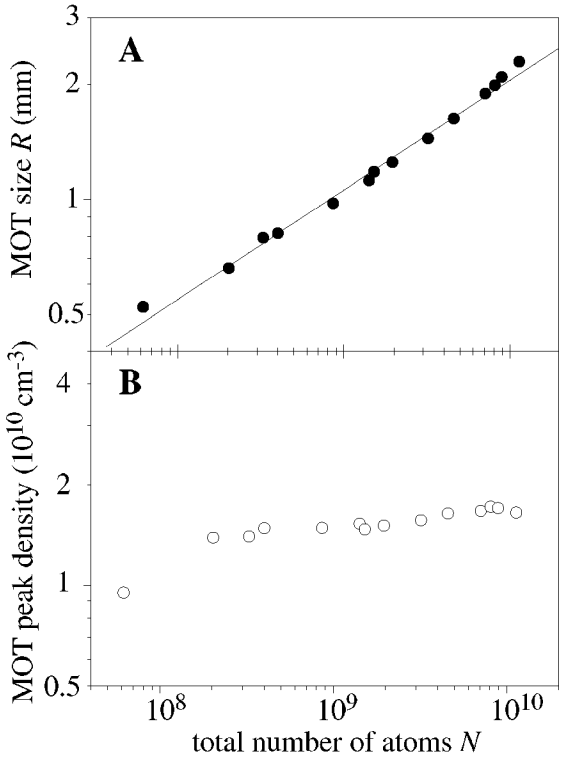

FIGURE 2. Experimental measurement of MOT size scaling law. The magnetic field gradient is $\nabla B = 10$ G/cm and the trapping light detuning $\delta = -2.5\Gamma$. The number of trapped atoms N is varied by adjusting the diameter of the repumper beam. We observe that the MOT size scaling law (**A**) is very close to $R \propto N^{1/3}$ throughout the whole range of N explored (the line is a fit yielding $R \propto N^{0.29}$). Accordingly, the peak atomic density in the MOT is independent of N (**B**).

The first term is the (unscreened) trapping force. The second term is the "multiple scattering force" which is due to the competition between the two effects (compression + repulsion) described above. The G_3 coefficient is positive in the case of a net repulsion. The equilibrium solution corresponds to $F(r) = 0$ everywhere inside the MOT yielding a constant spatial density $n = \kappa/G_3$. As n is fixed, adding more atoms to the MOT yields an increasing size R:

$$R \propto N^{1/3} \ . \tag{3}$$

This expansion of the MOT with increasing N is widely recognized as the signature of the multiple scattering regime for MOT operation. The dependence given by eq. 3 was reported for $N > 10^5$ by the authors of [7]. For even larger N ($> 5 \times 10^7$) they also reported an unexplained deviation from this model, with a MOT size increasing as $N^{1/2}$. One of the objectives of our study is to investigate the MOT scaling law in the regime of

wnloaded 16 Jul 2013 to 193.48.228.35. This article is copyrighted as indicated in the abstract. Reuse of AIP content is subject to the terms at: http://proceedings.aip.org/about/rights_permissi

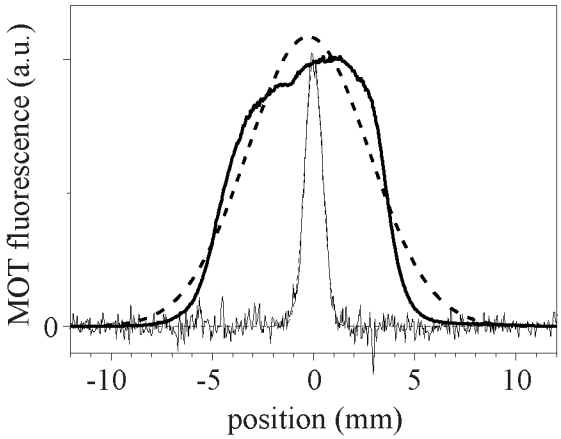

FIGURE 3. Density profiles of MOTs (experiment). We compare the (scaled) density profiles at "small" $N \approx 6 \times 10^7$ (thin solid curve) and at large $N \approx 10^{10}$ (bold solid curve). The parameters are the same as in Fig. 2. For small N the density is well fitted by a Gaussian (thin dashed line) while for large numbers of atoms the profiles are typically steeper in the edges and flatter at the top (the Gaussian fit is the bold dashed line).

large $N \gg 10^8$.

We now report in Fig. 2 our measurements of the MOT expansion with increasing N. The quantities characterizing the MOT (size R, number of atoms N, density n) are measured using the techniques described before. In Fig. 2 the number of trapped atoms is varied by changing the *diameter* of the repumper beam. In **A** we observe that the measured MOT expansion (symbols) follows a power law very close to $R \propto N^{1/3}$ (the line is a fit to N^{α} yielding $\alpha = 0.29$) for the whole range $5 \times 10^7 \leq N \leq 10^{10}$. Fig. 2**B** shows the measured peak atomic density, which is accordingly rather independent of N as expected from the model of [7]. These observations, resulting from the careful measurement procedure detailed in the experimental section, thus seem to corroborate this model even in our range of large N (at least with our MOT parameters).

Another prediction of the simple model of [7] is the *uniform* density profile of the MOT, a consequence of the linear spatial dependence of all forces involved. The authors of [7] reported observations confirming this prediction. We show in Fig. 3 two examples of density profile, corresponding respectively to the lowest (thin curve) and highest (bold curve) N values of Fig. 2. We observe that the low-N profile is well fitted by a Gaussian (thin dashed line), while the high-N one is quite steeper, with a flatter top (the bold dashed line is the gaussian fit). We stress again that these profiles are integrated along the line of sight. While the high-N profile is not clearly incompatible with a uniform 3D density, the Gaussian shape of the low-N cloud is expected only the temperature-limited regime i.e. for N even much lower.

Fig. 4 emphasizes the complexity of the situation in a MOT with a large ($> 10^8$) number of atoms. There, one can not in principle neglect the spatial dependence of the cross-sections $\langle \sigma_L \rangle$ and $\langle \sigma_R \rangle$, because of the spatially-varying Zeeman shift and laser

wnloaded 16 Jul 2013 to 193.48.228.35. This article is copyrighted as indicated in the abstract. Reuse of AIP content is subject to the terms at: http://proceedings.aip.org/about/rights_permissi

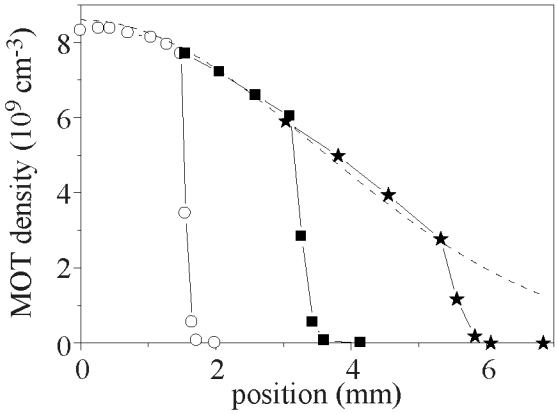

FIGURE 4. Density profile of a large MOT (numerical). We compute the MOT density profile for different numbers of trapped atoms: $N = 3.5 \times 10^8$ (circles), $N = 2.8 \times 10^9$ (squares) and $N = 8.8 \times 10^9$ (stars). The solid lines are shown to guide the eye. The MOT parameters are that of Fig. 2. We find truncated Gaussian density profiles, with a truncation radius increasing with N (while the Gaussian remains fixed, dashed line).

intensities. One must then relax the assumption of position-independent cross-sections which is employed in the analytical model of [7]. We thus developed a numerical model which employs a test-particle method, mainly to analyze the dynamical instabilities observed for large MOTs [15, 16] and discussed in the next section. This model allows us to compute the density profiles in Fig. 4 for different values of N, using the MOT parameters of Fig. 2. We see that these profiles correspond to truncated Gaussians, with a truncation radius increasing with N (note however that the width of the Gaussian itself is independent of N). In the limit of N small yielding a truncation radius much smaller than the Gaussian half-width, one recovers a quasi-uniform profile close to the prediction of [7].

The scaling law obtained in these conditions is $N^{1/3}$, as illustrated in Fig. 5. Here, the calculated MOT size R (circles) is plotted as a function of N (circles), in the conditions of Fig. 2. The observed dependence $R(N)$ is very close to the $N^{1/3}$ prediction of [7] (line). The slight deviation at N large is attributed to the proximity of the dynamical instability threshold [15, 16] (see next section). Directly comparing the measured density profiles to that of Fig. 4 is difficult since the measured profiles are integrated along the line of sight. We stress however that the measured profile of Fig. 3 (bold curve) is qualitatively compatible with both the 3D truncated Gaussian of Fig. 4 and the homogeneous density of [7]. Clearly, separating the two shapes would require a much more careful investigation.

To summarize, we have observed a $N^{1/3}$ scaling law for the MOT size in the range $5 \times 10^7 < N < 10^{10}$. This is qualitatively in agreement with the model of [7], although a numerical model reveals possible signatures of more subtle effects (e.g. position-dependent cross-sections) in the shape of the density distribution. It should be mentioned that we have also realized similar experiments, but varying N by adjusting the *intensity*

wnloaded 16 Jul 2013 to 193.48.228.35. This article is copyrighted as indicated in the abstract. Reuse of AIP content is subject to the terms at: http://proceedings.aip.org/about/rights_permissi

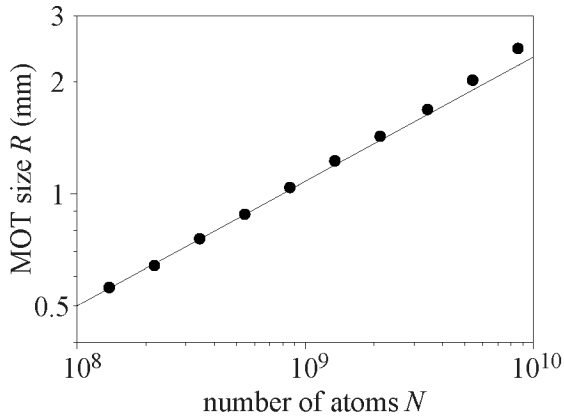

FIGURE 5. MOT scaling law (numerical). We calculate (circles) the MOT size R versus N, with the parameters of Fig. 2. The observed scaling law is close to $N^{1/3}$ (line).

of the repumping laser (see the experimental section). There, the results are quite different with a crossover between two distinct power laws. These data can not be fully explained even using the refined model of [12] which accounts for a varying population p in the bright state. We believe that a new effect could be involved, namely the repulsive interaction due to *repumping* photons. These observations will be reported in a forthcoming publication [17].

COLLECTIVE INSTABILITY IN LARGE MOTS

In the previous section we discussed the increase of the MOT size R with the number of trapped atoms N, which is widely accepted as a signature of the repulsive long-range interaction induced by scattering and reabsorption of photons by the atoms (multiple scattering regime). In the present section, we show that beyond a critical number of atoms N_{crit}, these interactions lead to the onset of an unstable behavior of the MOT.

It should be mentioned that spontaneous dynamical instabilities have already been observed in a MOT [9]. Characterized by center-of-mass oscillations, this instability occurs in a retro-reflected MOT because of the intensity *imbalance* between counter-propagating trapping beams. Indeed, the shadow effect is responsible for the attenuation of the laser passing through the cloud of atoms before being retro-reflected. Our case is qualitatively different, because our MOT is symmetric (no imbalance) and the independent beams configuration (instead of retro-reflected) removes the coupling between counter-propagating pairs and thus the feedback mechanism for the instability.

We first present an experimental study of this phenomenon. We then discuss a simple analytic model able to predict the threshold of the instability. A more involved numerical model, already presented in the previous section, allows us to confirm the threshold prediction and to investigate the dynamics of the MOT in the unstable regime.

wnloaded 16 Jul 2013 to 193.48.228.35. This article is copyrighted as indicated in the abstract. Reuse of AIP content is subject to the terms at: http://proceedings.aip.org/about/rights_permissi

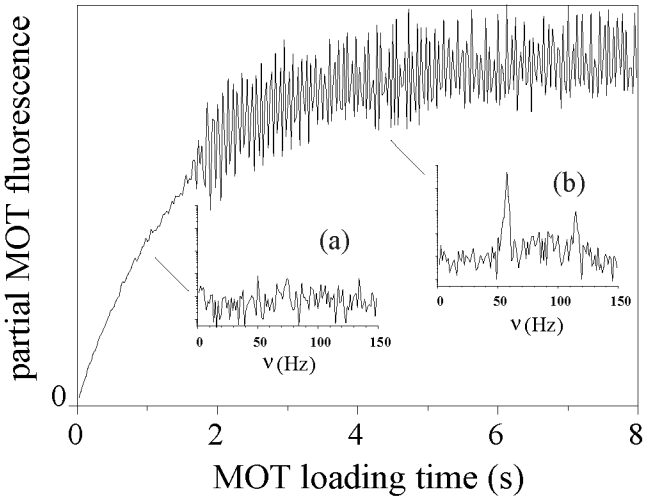

FIGURE 6. Direct observation of the MOT instability. We monitor the fluorescence of a portion of the MOT versus time after switch-on. The number of trapped atoms increases exponentially until a critical value N_{crit} (reached at $t \approx 1.7$s), where spontaneous, self-sustained oscilations of the trap volume set in. The difference between the stable regime $N < N_{crit}$ and the unstable one $N > N_{crit}$ is illustrated by the signal FFT's in insets (a) and (b) respectively.

Experimental study

Fig.6 provides an illustration of the onset of the collective instability. In this experiment [15], we record the light emitted by a portion of the MOT as a function of the time elapsed after the MOT has been switched on. The detected signal is roughly proportional to the number of atoms within the imaged volume. After the MOT is turned ON (at t=0), the number N of trapped atoms increases exponentially towards its steady-state value, determined by the parameters of the MOT. As discussed before, the MOT size increases smoothly with N without any specific dynamical features, as confirmed by the spectrum of the signal (inset (a)). When N reaches a certain critical value (here after ≈ 1.7 s), the MOT abruptly switches to a regime of self-sustained oscillations with a rather well-defined frequency (inset (b)). Here, the transition is observed by varying N for fixed MOT parameters (δ, ∇B, ...) which is the best illustration of the collective nature of this phenomenon. However, the instability threshold can also be crossed by tuning e.g. δ (see Fig. 8).

This existence of this unstable regime is found to be very robust: we observed it with different MOT setups and different atomic species (Rb^{85} and Rb^{87}, Sr^{88} [18]). It is also rather insensitive to the alignment of the MOT, although the details of the dynamics such as e.g. the spectrum (b) in Fig. 6 are alignment-dependent. The only necessary conditions for the instability seem to be: (1) a large number of trapped atoms (2) a rather small value of the trapping laser detuning ($|\delta| \approx \Gamma$ or below). This observation can be rendered more quantitative by plotting an "instability chart" for the MOT, such as

wnloaded 16 Jul 2013 to 193.48.228.35. This article is copyrighted as indicated in the abstract. Reuse of AIP content is subject to the terms at: http://proceedings.aip.org/about/rights_permissi

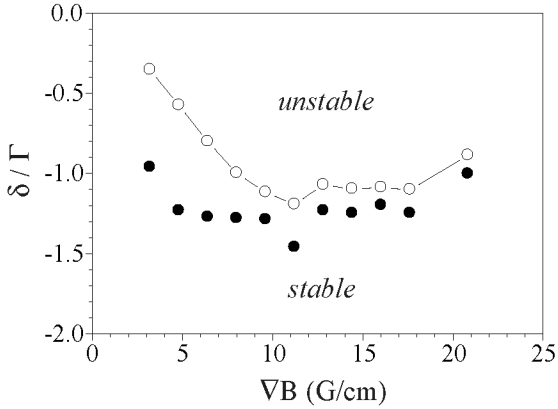

FIGURE 7. Instability chart of the MOT. We measure experimentally (solid symbols) the detuning δ at the instability threshold, for various value of the magnetic field gradient ∇B. Independently of ∇B, the MOT is unstable for $|\delta| \approx \Gamma$. The open circles are obtained using a simple analytic model (see text).

shown in Fig. 7. This chart is obtained in the following way: we vary the magnetic field gradient ∇B of the MOT, and for each value we adjust the detuning δ of the trapping laser to reach the instability threshold. The corresponding value of δ is reported (solid symbols) in Fig. 7. The threshold is determined by monitoring the *rms* fluctuations of the fluorescence signal of Fig. 6 (see the example of Fig. 8). It should be noted that the instability threshold also *a priori* depends on other MOT parameters such as e.g. the trapping laser intensity.

Since this experiment is performed in steady-state operation of the MOT, varying δ and ∇B affects the capture range and thus the number of trapped atoms. Thus, along the threshold border of Fig. 7 N and R do vary by as much as a factor 4 and 3 respectively. However, we monitored the transmission of the trapping beams through the MOT, and found it to be constant at $T \approx 0.4$ which corresponds to an optical thickness $b = -ln(T)$ close to unity. This seems to be a necessary condition for the instability to set in. We stress, however, that this condition is not sufficient since it can also be satisfied in the stable regime. By carefully monitoring N as a function of time during the oscillations (for a fixed set of MOT parameters), we found that the number of atoms is constant. This is a qualitative difference with the oscillations of [9], where the instability relies on a coupling between N and the center-of-mass position of the MOT.

We further investigated the MOT behavior near the threshold in order to determine the nature of the bifurcation. Fig. 8 shows the variation of the *rms* amplitude of the oscillations as the threshold is crossed by decreasing $|\delta|$. The variation is continuous across the threshold and shows no hysteresis. The threshold value is determined by a linear extrapolation of the oscillation amplitude to zero as pointed by the arrow. We also performed some measurements of the MOT oscillations after a small temporal "step" in the value of δ, and compared the situation just above and just below threshold. An example is show in Fig. 9: below threshold the MOT oscillation is damped while above

wnloaded 16 Jul 2013 to 193.48.228.35. This article is copyrighted as indicated in the abstract. Reuse of AIP content is subject to the terms at: http://proceedings.aip.org/about/rights_permissi

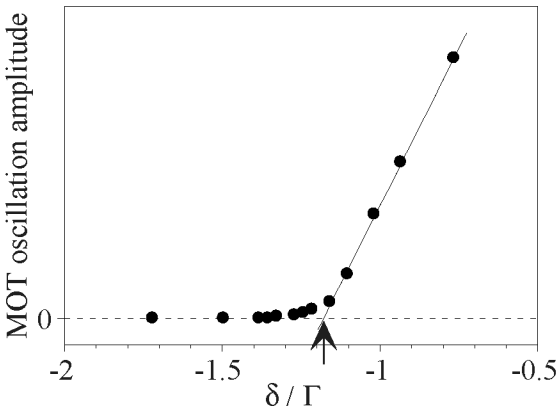

FIGURE 8. MOT oscillation across the instability threshold. We measure experimentally (circles) the *rms* amplitude of spontaneous MOT oscillations as the detuning is varied. This amplitude varies continuously across the transition. The instability threshold is determined using a linear extrapolation to zero amplitude (arrow).

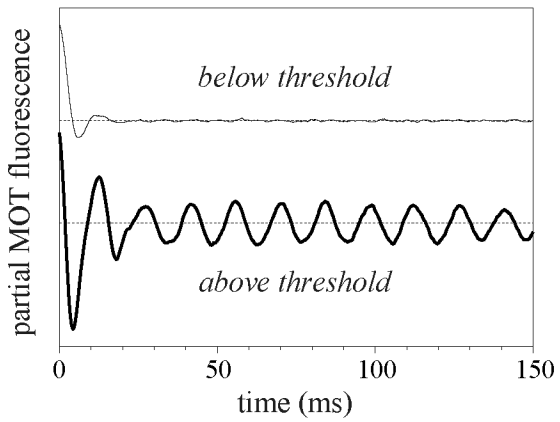

FIGURE 9. MOT relaxation above and below threshold. We measure the temporal evolution of the MOT partial fluorescence after a small "step" of δ at $t = 0$. Just below threshold (thin curve) the oscillation is rapidly damped, while it survives much longer just above threshold (thick curve).

threshold it survives for a long time without decaying. In this experiment we tune δ to cross the threshold. By fitting these curves with the function $f(t) = e^{-t/\tau} sin(\omega t + \phi)$, we can extract the damping time τ and the oscillation (angular) frequency ω. By measuring τ as a function of N when approaching the threshold, one could obtain the critical exponent of the bifurcation given by $\tau \propto (N_{crit} - N)^{-\gamma}$. This is done numerically in the following (see Fig. 10), using the model introduced in the previous section.

By performing the comparison of Fig. 9 for different values of ∇B, we observed that

wnloaded 16 Jul 2013 to 193.48.228.35. This article is copyrighted as indicated in the abstract. Reuse of AIP content is subject to the terms at: http://proceedings.aip.org/about/rights_permissi

the oscillation frequency in the unstable regime is closely related to that of the stable MOT (after excitation). All these observations are consistent with a supercritical Hopf bifurcation, a conclusion that will be confirmed by the numerical model.

Simple analytical model

We first developed a simple analytical approach, which helps to grasp the physical ingredients at work in this instability mechanism. In this 1D model, an atom located *outside* of the MOT at a location $x > R$ with a velocity v is subjected to the following force:

$$\begin{aligned} F(x,v) &= \frac{\hbar k\Gamma}{2} s_{inc}\{\frac{e^{-b}}{1+4\left[(\delta-\mu x-kv)/\Gamma\right]^2} \\ &- \frac{1}{1+4\left[(\delta+\mu x+kv)/\Gamma\right]^2} \\ &+ \frac{\eta}{1+4(\delta/\Gamma)^2}(1-e^{-b})(\frac{R}{x})^2\} \,. \end{aligned} \tag{4}$$

The first two terms on the right-hand side are due to the trapping laser beams. These expressions rely on the Doppler cooling theory, where we have accounted for the attenuation e^{-b} of the beam which passed through the cloud. It thus includes the compression force introduced in the previous section. s_{inc} is the on-resonance saturation parameter proportional to the intensity of the trapping beams. $\mu\nabla Bx$ is the Zeeman shift at position x. The third term in eq. 5 corresponds to the outward pointing radiation pressure originating from the light scattered by the atoms of the MOT. Using Gauss theorem, this "rescattering" force decays as $1/x^2$ outside of the MOT. A photon conservation argument yields that the total radiated power has to be $\propto 1-e^{-b}$ which measures the power depletion in the trapping beam. The coefficient η is the ratio of absorption cross-sections for rescattered and laser photons respectively. We now perform a linear stability analysis at the edge of the MOT $x = R$, which yields the instability condition:

$$e^{-b}\frac{\delta-\mu\nabla BR_{crit}}{1+\frac{4(\delta-\mu\nabla BR_{crit})^2}{\Gamma^2}} + \frac{\delta+\mu\nabla BR_{crit}}{1+\frac{4(\delta+\mu\nabla BR_{crit})^2}{\Gamma^2}} = 0 \,. \tag{5}$$

Under our experimental conditions, the expression simplifies to:

$$R_{crit} \approx \frac{|\delta|}{\mu\nabla B} \,. \tag{6}$$

We thus end up with a very simple prediction: the instability described in this paper is observed for MOTs with a radius such that the Zeeman shift at the edge ($\mu R\nabla B$) compensates the trapping laser detuning δ. We stress that this condition is not usually fulfilled in standard ($N <$ few 10^9) MOTs. With the typical values $\nabla B = 10$ G/cm and $\delta = -\Gamma$ eq. 6 yields $R_{crit} \approx 4$ mm which is quite larger than usual MOT sizes. This

wnloaded 16 Jul 2013 to 193.48.228.35. This article is copyrighted as indicated in the abstract. Reuse of AIP content is subject to the terms at: http://proceedings.aip.org/about/rights_permissi

size range is reached only for large numbers of trapped atoms $N > 10^9$ (see previous section). In Fig. 7 we plotted (open circles) the values of δ obtained with eq. 6 using the *measured* values of ∇B and R_{crit}. We see that the agreement is fair considering the extreme simplicity of our model.

More insight on the onset of the instability can be gathered by looking at the velocity dependence of the force at the edge of the MOT (eq. 5). One finds that when the threshold (6) is crossed, the friction $\partial F(x=R)/\partial v$ changes sign: the motion of atoms at the MOT edge is then accelerated instead of being damped, and these atoms are expelled outwards yielding an increasing MOT radius. Once the atomic density has decreased enough, multiple scattering effects vanish and the MOT resumes its usual, few atoms behavior. The atoms are thus pulled back towards the MOT center and the whole cycle starts over. This scenario is confirmed by the numerical simulations discussed in the next section, although we will see that the detailed dynamics is much more complex than anticipated by this simple one-zone model.

Numerical model

We discuss in the section the result of numerical simulations using a more refined, N-zone model [16]. The same model has been employed to study the MOT scaling laws. The simple model developed in the previous section has the merit to allow the understanding of the basic ingredients for the instability, and is even able to provide a reasonable prediction for the threshold. However, the complexity of the problem clearly requires a less trivial model, which will be adequate to quantitatively compare to the experiment. In particular, one has to relax the uniform density hypothesis implicitly used in the analytical model to be able to describe the full dynamics of the MOT in the unstable regime.

One application of the numerical model is the study of the critical regime. One can e.g. simulate the experiment of Fig. 9 and study the MOT relaxation after a small step in δ. The simulation yields a relaxation behavior quite similar to what is observed in the experiment (an example is provided in [16]). As mentioned earlier, one can then fit the relaxation curve by $e^{-t/\tau} sin(\omega t + \phi)$ and extract the damping time τ and the oscillation frequency ω. When approaching the instability threshold, one expects a divergence of τ. This is illustrated in Fig. 10(B) (circles), where the critical regime is explored by increasing N ($\delta = -1.5\Gamma$ and $\nabla B = 9$ G/cm). A fit by $\tau \propto (N_{crit} - N)^{-\gamma}$ (line) yields the critical exponent of the transition $\gamma = 0.55$, and the critical number of atoms at the bifurcation $N_{crit} = 1.226 \times 10^9$ (vertical dashed line). Fig. 10(A) shows the calculated MOT radius (solid circles) in the critical regime. The extrapolation to N_{crit} using a fitted power law (line) shows that the critical MOT radius R_{crit} is indeed well predicted by our simple analytical model (eq. 6, materialized by the horizontal dashed line).

The numerical model also allows us to explore the MOT dynamics deep inside the unstable regime. These predictions will be very useful to confront to future experiments investigating the details of the unstable MOT dynamics. An example is provided in [16] where we have calculated the temporal evolution of the atomic density profile above the instability threshold. This simulation qualitatively confirms the basic oscillation scenario

wnloaded 16 Jul 2013 to 193.48.228.35. This article is copyrighted as indicated in the abstract. Reuse of AIP content is subject to the terms at: http://proceedings.aip.org/about/rights_permissi

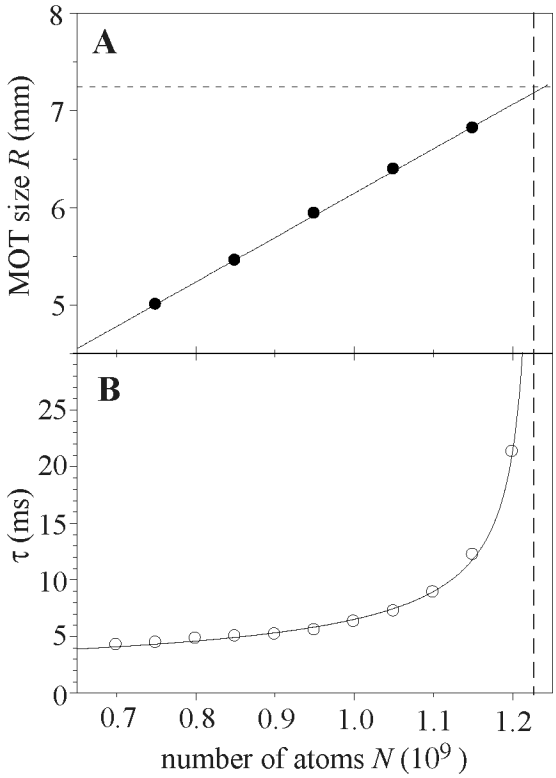

FIGURE 10. Critical behavior near the transition (numerical simulations). We compute in **B** the damping time τ (circles) versus the number of trapped atoms N near the critical value N_{crit}. A fit by $\tau \propto (N_{crit} - N)^{-\gamma}$ (line) yields the critical exponent $\gamma = 0.55$ and critical atom number $N_{crit} = 1.226 \times 10^9$ represented by the vertical dashed line. **A** shows the corresponding MOT radius R, whose critical value R_{crit} matches closely the prediction of the analytical model (horizontal dashed line).

discussed before, but also provides new insights on the details of the dynamics. The first observation is that the oscillation is far more complex than a simple "breathing mode". The cloud expansion is triggered by the driven motion of atoms located at the edge of the MOT, where the friction is negative. This is similar to what happens in pulsating stars, where the instability concerns an outer layer of the stellar envelope whose opacity varies and determines the impact of radiation pressure [1]. When bouncing back on the high density core of the cloud, these atoms excite a density wave propagating towards the MOT center where it is finally damped. The whole cycle can then resume. This process yields at a given time a quite complex density profile, which could possibly be investigated experimentally.

wnloaded 16 Jul 2013 to 193.48.228.35. This article is copyrighted as indicated in the abstract. Reuse of AIP content is subject to the terms at: http://proceedings.aip.org/about/rights_permissi

CONCLUSION

We have presented in this paper an overview of our investigations on long-range interactions in magneto-optical traps. The repulsive interaction arising from multiple light scattering inside the optically-thick MOT affects both its static and dynamic behaviors. In the standard (i.e. stable) mode of MOT operation, the scaling laws for the MOT size are determined by these light-induced interactions. We have investigated these scaling laws for a large number of trapped atoms ($10^8 < N < 10^{10}$). Our results qualitatively confirm the $N^{1/3}$ law derived in [7]. However, further observations suggest the possible role of the multiple scattering of *repumping* photons, a new mechanism which will be investigated in future experiments.

For N large and a relatively small detuning ($\delta \approx -\Gamma$) of the trapping laser, we have observed the onset of spontaneous, self-sustained oscillations of the MOT radius. This collective instability occurs via a supercritical Hopf bifurcation, as indicated by experimental observations and confirmed by numerical simulations. A simple analytical model based on the Doppler cooling theory allows to understand the basic mechanism responsible for this instability, which is different from that observed in MOTs so far. This model is also able to predict in a very simple form the instability threshold. A numerical model was developed to deal with the much more complex "real" situation in optically-thick MOTs. It not only confirms the physical interpretation and threshold prediction of the analytical model, but also yields original results such as the critical exponent at the transition and the details of the dynamics in the unstable regime. This model will be an invaluable tool to analyze the results of future experiments. Work in progress include e.g. the study of the critical regime and of the behavior of the MOT in the regime of forced excitation.

ACKNOWLEDGEMENTS

We acknowledge financial support by the CNRS, PACA region, and by NSF through a grant to ITAMP.

REFERENCES

1. J. P. Cox, *Theory of stellar pulsation* (Princeton University Press, Princeton, NJ, 1980).
2. U. Erdmann, W. Ebeling, and A. S. Mikhailov, *Phys. Rev. E* **71**, 051904 (2005).
3. M. P. Evrard *et al.*, *Plasma Phys.* **21**, 999 (1979).
4. J. J. Bollinger, T. B. Mitchell, X.-P. Huang, W. M. Itano, J. N. Tan, B. M. Jelenkovic, and D. J. Wineland, *Physics of Plasmas* **7**, 7 (2000).
5. C. E. Simien *et al.*, *Phys. Rev. Lett.* **92**, 143001 (2004).
6. T. Lahaye, T. Koch, B. Fröhlich, M. Fattori, J. Metz, A. Griesmaier, S. Giovanazzi, T. Pfau, *Nature* **448**, 672 (2007).
7. T. Walker, D. Sesko and C. Wieman, *Phys. Rev. Lett.* **64**, 408 (1990); D. W. Sesko, T. G. Walker, and C. E. Wieman, *J. Opt. Soc. Am. B* **8**, 946 (1991).
8. C. Monroe, W. Swann, H. Robinson, and C. Wieman, *Phys. Rev. Lett.* **65**, 1571 (19990); K. E. Gibble, S. Kasapi, and S. Chu, *Optics Lett.* **17** 526 (1992).
9. D. Wilkowski, J. Ringot, D. Hennequin and J.-C. Garreau, *Phys. Rev. Lett.* **85**, 1839 (2000); A. di Stephano, P. Verkerk, and D. Hennequin, *Eur. Phys. J. D* **30**, 243 (2004).

wnloaded 16 Jul 2013 to 193.48.228.35. This article is copyrighted as indicated in the abstract. Reuse of AIP content is subject to the terms at: http://proceedings.aip.org/about/rights_permissi

10. G. Labeyrie, D. Delande, C. A. Müller, C. Miniatura, R. Kaiser, *Opt. Commun.* **243**, 157 (2004).
11. E. L. Raab, M. Prentiss, A. Cable, S. Chu, and D. E. Pritchard, *Phys. Rev. Lett.* **59**, 2631 (1987).
12. W. Ketterle, K. Davis, M. Joffe, A. Martin, D. Pritchard, *Phys. Rev. Lett.* **70**, 2253 (1993).
13. M. H. Anderson *et al.*, *Science* **269**, 198 (1995); K. B. Davis *et al.*, *Phys. Rev. Lett.* **75**, 3969 (1995); C. C. Bradley, C. A. Sackett, J. J. Tollett and R. G. Hulet, *Phys. Rev. Lett.* **75**, 1687 (1995).
14. J. Dalibard, *Opt. Commun.* **68**, 203 (1988).
15. G. Labeyrie, F. Michaud, R. Kaiser, *Phys. Rev. Lett.* **96**, 023003 (2006).
16. T. Pohl, G. Labeyrie, R. Kaiser, *Phys. Rev. A* **74**, 023409 (2006).
17. G. L. Gattobigio, T. Pohl, G. Labeyrie, and R. Kaiser, submitted to *Phys. Rev. A*.
18. D. Wilkowski, *private communication*.

wnloaded 16 Jul 2013 to 193.48.228.35. This article is copyrighted as indicated in the abstract. Reuse of AIP content is subject to the terms at: http://proceedings.aip.org/about/rights_permissi